DOI:
10.1039/D3NR04862D

Document Version
Peer reviewed version

Nanoscale

Accepted Manuscript

This article can be cited before page numbers have been issued, to do this please use: A. Darumas Putri, M. Hsu, C. Han, F. Chao, C. Hsu, C. D. Lorenz and C. Hsieh, *Nanoscale*, 2023, DOI: 10.1039/D3NR04862D.

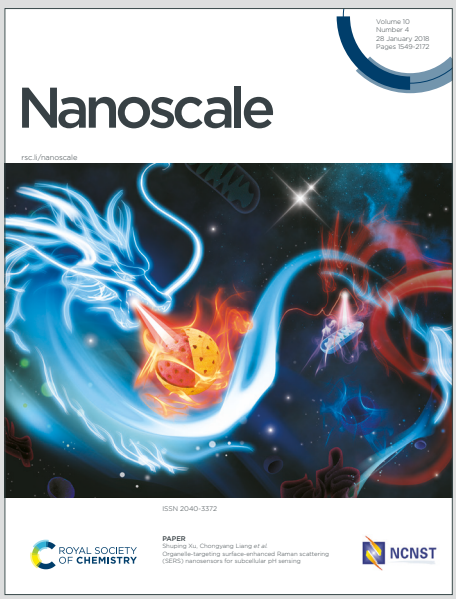

ROYAL SOCIETY OF CHEMISTRY

rsc.li/nanoscale

View Article Online
DOI: 10.1039/D3NR04862D

ARTICLE

Differential Cellular Responses to FDA-Approved Nanomedicines: An Exploration of Albumin-Based Nanocarriers and Liposomes in Protein Corona Formation

Received 00th January 20xx,
Accepted 00th January 20xx

DOI: 10.1039/x0xx00000x

Athika Darumas Putri[a,b#], Ming-Jen Hsu[c#], Chia-Li Han[d], Fang-Ching Chao[e], Chun-Hua Hsu[f], Christian D. Lorenz[g], and Chien-Ming Hsieh[a,h*]

Albumin nanoparticles (NPs) and PEGylated liposomes have garnered tremendous interest as therapeutic drug carriers due to their unique physicochemical properties. These unique properties also have significant effects on the composition and structure of the protein corona formed around these NPs in a biological environment. Herein, the protein corona formation on albumin NPs and liposomes was simultaneously evaluated through in vitro and simulation studies. The sizes of both types of NPs increased with more negatively charged interfaces upon being introduced into fetal bovine serum. Gel electrophoresis and label-free quantitative proteomics were performed to identify proteins recruited to the hard corona, and fewer proteins were found in albumin NPs than in liposomes, which is in accordance with isothermal titration calorimetry. The cellular uptake efficiency of both NPs significantly differed in different serum concentrations, which was further scrutinized by loading of an anticancer compound into albumin NPs. The presence of the hard protein corona increased cellular uptake of albumin NPs in comparison to liposomes. In our simulation study, a specific receptor present in membrane was greatly attracted to the albumin-apolipoprotein E complex. Overall, this study not only evaluated protein corona formation on albumin NPs, but also enhanced promising advancements toward albumin and liposomes-based therapeutic systems

Introduction

Protein corona formation on nanoparticles (NPs) is known to produce an unpredicted state that affects them once they are transported into the bloodstream; its formation is a result of various intrinsic factors that range from the physicochemical properties of the NPs to the current biological milieu of interest. Physical and chemical properties of NPs can be tuned in order to optimize the capability of a given NP to achieve its desired purpose, such as the targeted delivery of drugs[1, 2]. One factor that is important in controlling interactions of an NP with a biological environment is the nature of its surface chemistry. Studies revealed that several factors are directly affected by the surface chemistry of an NP, including ligand functionalization, the surface charge, and shape of the NP, which can affect cellular uptake due to the formation of a protein corona in plasma or serum[3]. For example, zwitterionic polymer NPs are preferred as drug-nanocarrier due to their excellent anti-fouling properties against non-specific *in vitro* and *in vivo* binding[4]. In another study, significantly larger amounts of immunoglobulins were identified on the rod-like shaped NPs than on spherical NPs, which showed a greater immune response thereafter leading to a different biological fate[5].

Protein NPs and liposomes have been widely used in biomedical and drug delivery applications for decades[6-8]. The significant impacts of their application in this field can be seen as they are among Food and Drug Administration (FDA)-approved delivery platforms. The presence of polyethylene glycol (PEG) was shown to decrease protein corona formation on NPs[9]. Notably, PEGylated liposomes used in the formulation of the anticancer chemotherapeutic drug, Doxil®, which includes 2-kDa PEG chains, produced drastic reduction of aggregation and opsonization which prolonged systemic circulation of the NPs[10]. However, some reports detected anti-PEG antibodies after the first *in vivo* dose[11-13]. This

[a.] *School of Pharmacy, College of Pharmacy, Taipei Medical University, Taipei, 11031, Taiwan.*
[b.] *Semarang College of Pharmaceutical Sciences (STIFAR), Semarang City, 50192, Indonesia.*
[c.] *Department of Pharmacology, Taipei Medical University, Taipei, 11031, Taiwan.*
[d.] *Master Program in Clinical Genomics and Proteomics, College of Pharmacy, Taipei Medical University, Taipei, 11031, Taiwan.*
[e.] *Université Paris-Saclay, CNRS UMR 8612, Institut Galien Paris-Saclay, Châtenay-Malabry, France.*
[f.] *Department of Agricultural Chemistry, National Taiwan University, Taipei, 10617, Taiwan.*
[g.] *Biological Physics and Soft Matter Group, Department of Physics, King's College London, London WC2R 2LS, United Kingdom.*
[h.] *Ph.D. Program in Drug Discovery and Development Industry, College of Pharmacy, Taipei Medical University, Taipei, 11031, Taiwan.*
#ADP and MJH contributed equally to this work.
Electronic Supplementary Information (ESI) available: [details of any supplementary information available should be included here]. See DOI: 10.1039/x0xx00000x

immunogenic response was considered to be due to the PEGylation of the liposome surface. Indeed, most current studies explored the function of the protein pre-adsorption of developed NPs prior to biological examination, which means that the protein present could be a versatile mechanism to disguise the recognition of the NP core by the immune system[14-16]. It is worth noting that under similar conditions, both protein NPs and liposomes may regulate different complexities of corona proteins during residency within each biological milieu.

In this study, we investigated the effect of serum and protein corona formation on interactions of albumin NPs and liposomes with their cellular environment, MIA PaCa-2 cancer cells, and macrophages. Human serum albumin (HSA) was employed as the protein-based NPs and prepared via two-step emulsification based on NP albumin-bound (NAB) technology. Cationic liposomes, as an example of nanocarrier approved for messenger (m)RNA therapeutics, were utilized as a positively charged model for comparison with albumin NPs[17]. We examined various nanoparticle (NP) responses to serum and evaluated the impact of hard corona formation on cellular interactions. To our knowledge, no previous study has directly compared these two NP types. Here, we emphasize that the hard protein corona notably increases cellular uptake of albumin NPs compared to liposomes. The binding affinity of albumin NPs with proteins found within the protein corona and the internalization mechanism that cells used for these NPs were further evaluated using coarse-grained molecular dynamic simulations.

Experimental

HSA NPs preparation

Albumin NPs were prepared using the emulsion-solvent evaporation method with a high-pressure homogenizer (HPH). Initially, a 1% v/v emulsion of HSA was prepared in double-distilled water (DDW). Separately, soybean lecithin (135 mg) was dissolved in chloroform/ethanol (9:1) using an ultrasonic bath at 50°C. The soybean lecithin solution was then incorporated into the HSA emulsion through ultrasonication, which was carried out for 5 min with amplitude set to 30% (ultrasonic oscillation; VCX 750, frequency: 20 kHz, Sonics and Materials, Newtown, CT, USA), followed by treatment with HPH (NanoLyzer-N2, Cogene, Hsinchu, Taiwan) at a pressure of 20,000 psi. After one cycle, the nano-sized emulsion was collected. The organic solvent was subsequently removed from the emulsion using rotary evaporation under reduced pressure and elevated temperature. The resulting NPs were filtered using a 0.2 µm-regenerated cellulose membrane to eliminate unbound drugs and impurities. Trehalose was added to the NPs, which were then freeze-dried and stored at 4°C. In the case of drug incorporation (30 mg MPT0B291), the preparation followed a similar process with the soybean lecithin solution in chloroform/ethanol, as described in a previous study[18].

Liposomes preparation

All lipids (cholesterol: 1,2-dioleoyl-3-trimethylammonium propane (DOTAP): dioleoylphosphatidylethanolamine (DOPE): 1,2-distearoyl-sn-glycero-3-phosphorylethanolamine (DSPE)-PEG = 30:50:19:1, mol: mol) were dissolved in chloroform in round flask and gently vortexed for 5 min. Chloroform was rotary-evaporated under low vacuum (500 mmHg) for 40 min at 50~60 ℃ to completely remove the organic solvent. Afterward, DDW (1.5 mL) was added to hydrate the resulting lipid film, followed by gentle vortexing until the suspension was homogenized. The suspension was passed through the polycarbonate membrane (size = 100 nm; Avanti Polar Lipids, Inc.) 11 times in an extruder (Avanti Polar Lipids, Inc.) with two 1.0 mL-glass syringes. The resulting liposomes were stored at 4℃ and used within 1 month[19].

Particle size and particle charge measurements

A dynamic light scattering (DLS) analysis was conducted using the Zetasizer Nano S90 DLS system (Malvern Panalytical Ltd.). Triplicate consecutive measurements were collected and averaged as representative results. The laser power settings and time required for acquisition of each measurement were set by default according to the software. Both albumin NPs (lyophilized) and liposomes were prepared in DDW, diluted to 10 µg mL^{-1}, and measured at 25℃ with scattered light detected at a 90° angle. The resulting data were processed using Zetasizer Software. Average particle sizes were determined by the weighted intensity of the scattered light. Similar instrument and sample procedures were employed to evaluate the zeta potential (ζ-potential) of both types of samples. Disposable folded capillary cells were used in this measurement.

Protein corona formation

Albumin NPs (~1.5 mg mL^{-1}) or liposomes (~1.0 mg mL^{-1}) were incubated with 50% or 15% fetal bovine serum (FBS) in a 1:1 ratio for 1 h at 37℃. The unbound and free proteins were washed away with several centrifugation steps. Both NPs were centrifuged three times at 15,570 *×g* (**Supplementary Fig. S1**). In each centrifugation wash, the supernatant was collected and the pellet was washed with DDW and placed into a new Eppendorf tube. The final pellet was resuspended in DDW (100 µL). Concentrations of the NPs with protein corona and supernatants were determined with a bicinchoninic acid (BCA) assay (**Scheme S1**).

Gel electrophoresis of protein corona

Both NP pellets with protein corona (20 µg of proteins) and the collected supernatants of each wash were mixed with 4X sample buffer solution and incubated for 5 min at 95℃ upon being added to a 10% sodium dodecylsulfate (SDS)-polyacrylamide gel electrophoresis (PAGE) gel. The resulting solutions along with a protein ladder were applied for gel-electrophoresis and run at 100 V for about 90 min. The resulting gels containing separated proteins were stained with

View Article Online
DOI: 10.1039/D3NR04862D

Coomassie blue and silver-stain for analyses. In order to measure the intensity of each molecular-weight band, Fiji (ImageJ) software was employed for molecular-weight and densitometric analyses.

NanoLC-ESI-MS/MS analysis

The protein corona sample was treated overnight by our previously reported gel-assisted trypsin digestion[20] before being examined in duplicate with the Ultimate system 3000 nanoLC system (Thermo Fisher Scientific) linked to an Orbitrap Fusion™ Lumos™ Tribrid™ Mass Spectrometer (Thermo Fisher Scientific). Peptides were placed into 75-µm inside diameter, 25 cm C18 Acclaim PepMap NanoLC column (Thermo Fisher Scientific) compacted with 2-µm particles (with a pore size of 100 Å). Collected peptides were then eluted in the mobile phase used within the run (composed of 0.1% formic acid in acetonitrile) at 0% ~ 35%. The flow rate was 300 nL min^{-1}. The entire analysis was accomplished within 120 min.

The data-dependent acquisition mode was employed to carry out the LC-MS experiment. A full-scan MS and subsequent MS/MS were consecutively scheduled within 3-second cycle period. Full MS scans were obtained in the Orbitrap from m/z 350 to 1700. The resolution used was 120,000. The maximum ion injection time was set to 50 ms or with an automatic gain control of 5E5.

The precursor with assigned charge states spanning 2+ to 5+ was sequentially isolated for HCD with normalized collision energy of 32%. Further, a resolution of 60,000 was applied in the MS/MS scan to capture the fragmented ions in the Orbitrap. The automatic gain control (AGC) was subsequently set to 5E4 or executed using a maximum ion injection time of 50 ms. Within 180 s, the previously obtained precursors were dynamically omitted from reacquisition.

Proteome identification and quantitation

The protein corona was identified by searching MS raw files using the SwissProt bovine protein sequence database (vers. 2022.05, sequence 6961) using MaxQuant[21]. Oxidation (Met), acetyl (N-term Protein), and deamidation (Asn, Gln) were assigned as variable modifications, while methylthio (Cys) was assigned as a fixed modification. Mass tolerances were set to 20 ppm for the peptide precursor and 0.1 Da for the fragment ion. Only tryptic peptides with at least seven amino acids and a maximum of two missed cleavages were permitted. A false discovery rate (FDR) of 1% was applied to the peptide spectral match (PSM) and protein level.

We further filtered differentially expressed proteins using normalized spectral counts as intensity percentages ($NpSpC_k$) among protein coronas from two NP types at different serum concentrations. The molecular weight of each identified protein in the LC-MS/MS analysis was retrieved using UNIPROT. Afterward, relative concentrations of detected proteins were calculated with the following formula[22]:

$$NpSpC_k = \left(\frac{(SpC/(MW)_k)}{\sum_{t=1}^{n}(SpC/(MW)_t)}\right) \times 100$$

where *SpC* refers to the peptide spectra count detected by LC-MS/MS, and *k* and *MW* respectively represent each protein and its molecular weight (Da).

Cell viability study

The effect of protein serum on the cytotoxicity of MPT0B291-albumin NPs was determined in MIA PaCa-2 cells using MTT assays. Herein, serum-free media and media containing 15% or 50% serum (using FBS; denoted as "serum") were employed to treat drug containing-albumin NPs (i.e., MPT0B291 drug[23]). Drug concentrations in the NPs were prepared by serial dilutions spanning 0.001 to 100 µg mL^{-1}. Briefly, MIA PaCa-2 cells were seeded (7×10^3 cells/well) in 96-well culture plates for 24 h in a humidified incubator at 37°C with 5% CO_2. Afterward, the medium of the adherent cells was replaced with drug concentrations diluted in serum-free media or media with specific serum concentrations (15% or 50% serum) and incubated for 24 h. Cells were then treated with an MTT solution (100 µL, 500 µg mL^{-1} in 1X phosphate buffer saline (PBS; pH 7.4)) and incubated at 37°C for 2 h. The medium was then removed, followed by adding DMSO (100 µL) to each well to dissolve the formazan crystals. The optical density (OD) was read at 570 nm using microplate reader (Cytation™ 3 Cell Imaging Multi-Mode Reader, BioTek, USA). The cell survival rate was calculated as follows:

$$Cell\ survival\ rate\ (\%) = \frac{OD\ value\ of\ test\ solution\ group}{OD\ value\ of\ control\ solution\ group} \times 100\%$$

Cell uptake study (internalization)

3,3-Dioctadecyloxacarbocyanine (DiO) perchlorate was employed and dissolved in a chloroform/ethanol (9:1) solution to a final concentration of 1 mg mL^{-1}. The process to incorporate the DiO into albumin NPs was then conducted in a similar way to the drug-encapsulated albumin NPs. After a final evaporation step, the nanoemulsion was filtered through a 0.2-µm of regenerated cellulose membrane. NP sizes were determined using the above-described procedures. The internalization study was done by firstly plating the MIA Paca-2 cells (10^5 cells/well) onto 12-well plates. NPs were prepared against different conditions of serum-containing media. For the experiment of direct incubation, NPs were directly introduced into serum-containing media without prior incubation outside the cells. Meanwhile, for the experiment to evaluate the effect of incubation time with serum proteins, NPs were incubated for 1 h with the serum-containing media before they were added to cells. In regards to the experiment involving hard-corona proteins, unbound and free proteins were separated from bound proteins through centrifugation at 15,570 ×*g* for 1 h. The final pellet was collected, and the protein concentration was checked. The NP-hard corona protein complex at 1 µg mL^{-1} was then introduced to cells and incubated for 24 h. Cells were evaluated using a microplate reader (Cytation™ 3 Cell Imaging Multi-Mode Reader, BioTek, USA) to elucidate the internalization process.

Cell uptake study (flow cytometry)

DiO perchlorate was used by dissolving it in a chloroform/ethanol solution (9:1) to a final concentration of 1 mg mL^{-1}. DiO was incorporated into albumin NPs in a way similar to that of drug-encapsulated albumin NPs. After a final evaporation step, the nanoemulsion was filtered through a 0.2-µm regenerated cellulose membrane. NPs size was determined using the above-described procedures. The internalization study was done by first plating MIA Paca-2 cells (10^5 cells/well) onto 12-well plates. NPs were prepared against different conditions of serum-containing media in a 1:1 ratio. The NP-hard corona protein complex at 1 µg mL^{-1} was introduced to cells and incubated for certain periods of 1, 2, and 8 h. After each incubation, 1 mL of trypsin was added to detach cells, followed by adding an extra 1 mL of fresh medium for collection. Cells were washed with ice-cold PBS three times and processed for flow cytometry reading. Then 10,000 cells were counted for DiO signal collection. Debris or non-specific cellular fragments were neglected from the analysis by creating a gate with the most populated cells according to side-scatter versus forward-scatter axes.

Coarse-grained molecular simulation setting

The HSA protein (protein data bank (PDB): 2BXA) was employed as a template for protein modelling due to its high relatedness with BSA sequences, and it was prepared using SWISS Dock-Prep. The protein was refined for missing residues and undistributed charges. Similar procedures were used for the other proteins, apolipoprotein C3 (PDB: 2JQ3), apolipoprotein E (PDB: 1LPE), low density lipoprotein receptor (LDL-R; PDB: 1N7D), and complement C3 (PDB: 2QKI). All the proteins were examined using Discovery Studio Visualizer and Swiss PDB Viewer to complete the missing residues.

Coarse-grained simulations were performed using the GROMACS package (Version 2019) and the Martini (Version 2.1) forcefield[24, 25](the details of MD simulations used were as suggested by MARTINI developers). The time step used was 20 fs with Verlet neighborlist scheme employed based on energy drift tolerance. Coulomb interaction was treated using reaction field and electrostatic interaction used was 15. Thermostat used was 310 K with the coupling of velocity rescale (v-rescale) and the coupling constant in the order of 1.0 ps. The pressure was controlled using Parinello-Rahman barostat with compressibility of $3x10^{-4}$. In membrane layer, the pressure was controlled using semiisotropic. The water added was according to Martini topologies, where 4 molecules was considered as 1 coarse-grained bead. The counterions were added representatively with the additional ions to represent physiological environment of NaCl (0.15 M). The minimization stage was initially done using the steepest descent algorithm with 500 steps which was then followed by 9000 ps of equilibrium at 310 K. The production stage was performed afterward with the snapshots obtained every 1 ps.

To compute the PMF for the interaction of the system, the umbrella sampling approach was carried out. The restraint potential used the harmonic potential with force constant of 1000 kJ/mol.nm^2. Total of 40 simulation windows were performed with spacing of 0.1 nm and simulated for 8 ns. The PMF analyses were done by extraction of PMF using WHAM in GROMACS that yielded the ΔG from each system (albumin NP with protein). Number of bins used was 200, temperature of 310, and number of bootstrap of 100.

Coarse-grained molecular dynamics simulations of membrane-protein interaction

Coordinates of all atomistic proteins were employed to produce a coarse-grained model through 'martinize.py'[26]. Each protein was coarse-grained with an elastic bond force constant of 500 kJ mol^{-1} nm^{-2} and an upper cutoff of 0.9 nm[27]. The simulation temperature was set to 310 K. In order to elucidate the role of LDL-R on the membrane toward the apolipoprotein, molecular dynamic simulations with the Martini coarse-grain forcefield (considering the huge size of the system) were also conducted. Coarse-grain molecules of apolipoprotein and LDL-R were constructed in a similar way with the above protein protocol. After each system was run for several hundred nanoseconds (until reaching a stable system), each molecule was combined as a complex and a dynamic simulation was further processed.

A membrane system was built comprised of sphingomyelin, PC(1,2-dioleoyl-sn-glycero-3-phosphocholine) (DOPC), PE(1,2-dioleoyl-sn-glycero-3-phosphoethanolamine) (DOPE), PS(1,2-dioleoyl-sn-glycero-3-phospho-L-serine) (DOPS), and cholesterol in respective of 27 : 30 : 15 : 15 : 51, lipid content ratio[28]. The membrane composition was chosen to represent a cancerous model, as explained in previous findings by Rivel and coworkers[28]. A membrane size of 34×25×28 nm was generated with insane.py script and continued to a series of minimization and gradual equilibrations with time-steps of 40 fs, for up to 20 ns. To ensure equilibrium, the equilibration of the windows was assessed by comparing the positions of the protein-albumin nanoparticle in both the initial and final windows. If the positions were found to be similar, it indicated that the system had reached an adequate equilibrium.

The semi-isotropic Berendsen barostat was utilized for equilibration steps with a coupling constant of 6.0 ps[29]. The optimization process was done by running MD annealing of the protein-membrane complex, while maintaining the remaining structure. Afterward, a dynamic simulation was applied to the membrane with 30-fs of time-steps.

To incorporate LDL-R in the membrane (LDL-R/membrane), the protein was arranged to be approximately in the middle of the membrane with the binding site (epitopes) facing outward (i.e., the histone-rich region) by insane.py script and was similarly processed as mentioned above for minimization, equilibration, and dynamic runs. The corona complex was inserted and allowed to hover over the membrane at a 5-nm distance. The complex system was then run for minimization and equilibration before a dynamic run was conducted for 500 ns.

Results and Discussion

NP synthesis and protein corona formation

Both bare albumin NPs and liposomes were found to have similar sizes (of under 200 nm) with different original surface charges. The albumin NPs were negatively charged (anionic) as they are protein based, whereas liposomes were positively charged (cationic) due to the large amount of DOTAP[15]. Further, protein corona formation was then investigated by incubating the NPs in different serum concentrations (15% and 50% FBS) for 1 h.

The particle size and charge seemed to change upon being incubated in the higher serum concentration. Protein corona formation on the NP surface was clearly shown by the increase in the particle size when the NPs were placed in serum (**Table 1**). The presence of free proteins in both NP-serum systems was also possibly indicated by the small green peak in **Fig. S2** due to the agglomeration of free serum proteins during incubation[30-32]. Considering that both NPs were almost the same size with small variations, the surface area and any curvature might have had less effect on protein adsorption. The two NPs were shown to have distinct differences in surface charges before and after incubations with serum (**Table 1**). The albumin NPs became more negatively charged after protein corona formation, while the liposomes have remarkably changed from being positively charged to negatively charged, which confirmed that the accumulated charges of the protein corona concealed the original charge of the NPs.

Hard corona formation on the surface of each NP was investigated through gel electrophoresis. After incubation with serum, the NPs were collected and washed several times to remove free and unbound serum proteins through serial centrifugations[33]. Protein concentrations of the obtained pellets were determined using BCA assays followed by SDS-PAGE and image densitometric analyses to characterize the proteins that were found within the hard corona on the surface of each NP (**Fig. 1**). As shown in **Fig. 1**, albumin NPs recruited a smaller number of proteins to its corona as compared to liposomes. Meanwhile, several band peaks were greatly enhanced for liposomes in serum, while these bands were absent from results of albumin NPs, such as those at around 185 kDa, 140~160 kDa, and 27 kDa which were likely to be complement C3, alpha-2-macroglobulin, and apolipoprotein A-1, respectively (as also indicated by LC-MS/MS). In addition, free-liposome and serum-only lanes revealed the absence of proteins respectively indicative of no protein content and no remaining proteins present at the surface of the centrifuged serum pellet. Further, different serum concentrations caused variations in protein compositions which then affected the corona proteins that formed on each NP. For instance, the protein corona on albumin NP surfaces had a greater peak intensity at 130 kDa (i.e., thrombospondin-1 protein) upon incubation in high concentration of serum.

Although lipids in the liposomes were PEGylated, several distinct protein bands were observed to be higher in the liposome system compared to albumin NPs. These results were in accordance with the protein corona profile measured in other polymeric NPs containing PEG[34, 35]. Quaternary amines of DOTAP in liposomes contributed to the positive charges, while bare albumin NPs were associated with total net negative charges due to the albumin. These results implied that the accumulated charges associated with the particles, rather than the functionalized surface chemistry, such as PEG, played a significant role in inducing protein adsorption[36]. An increased band intensity of a given protein found in a complex of NPs in higher-concentration serum suggested that the particular corona protein may be found in a greater abundance in the higher-serum concentration as a result of having more-favorable interactions with the NP surface. Since most proteins in serum are negatively charged, the proteins were more likely to interact with the cationic liposomes rather than with anionic/neutral albumin NPs through electrostatic interaction[37, 38].

Table 1. Identification of protein corona formation on the albumin NPs and liposomes surfaces; the particle numbers of albumin NPs and liposomes were equally adjusted.

Nanoparticle complex	Size (nm)	Polydispersity index	ζ-potential (mV)
Albumin NPs only	128.9±11	0.284±0.066	-0.84±0.335
Albumin NPs-low serum	150.7±6	0.551±0.088	-10.45±1.540
Albumin NPs-high serum	190.2±4	0.271±0.081	-9.21±0.810
Liposomes only	117.3±0.4	0.116±0.013	48.3±4.300
Liposomes-low serum	149.9±2	0.145±0.015	-15±1.300
Liposomes-high serum	211.6±14	0.337±0.041	-18±0.265

Identification of the protein corona composition through a proteomics analysis

To quantitatively investigate the protein corona bound to the NPs, shotgun proteomics using LC-MS/MS were employed. We noted that it could be a challenge in albumin NPs to differentiate the albumin from the NPs and the albumin from the serum used. The albumin protein length identified by LC-MS/MS was further able to be classified to two different species through recognition of unique peptides under albumin of *Homo sapiens* (human serum albumin, HSA) and albumin of *Bos taurus* (bovine serum albumin, BSA) databases. BSA in this regard is known to share around 75% sequence homology with HSA[39, 40]. In terms of the stability, both BSA and HSA also possess the same disulfide bridges preserved across the residues[41]. It is also known that the two proteins induce different fluorescence signal during ligand binding[42, 43]. It further turned out that the two shared significantly diverse sequences of important residues on the loop linking the IIA and IIB subdomains and several residues on the IIB subdomains[39]. In order to distinguish the same type of protein shared by two different species, we searched for specific residues or unique peptides contained in each species.

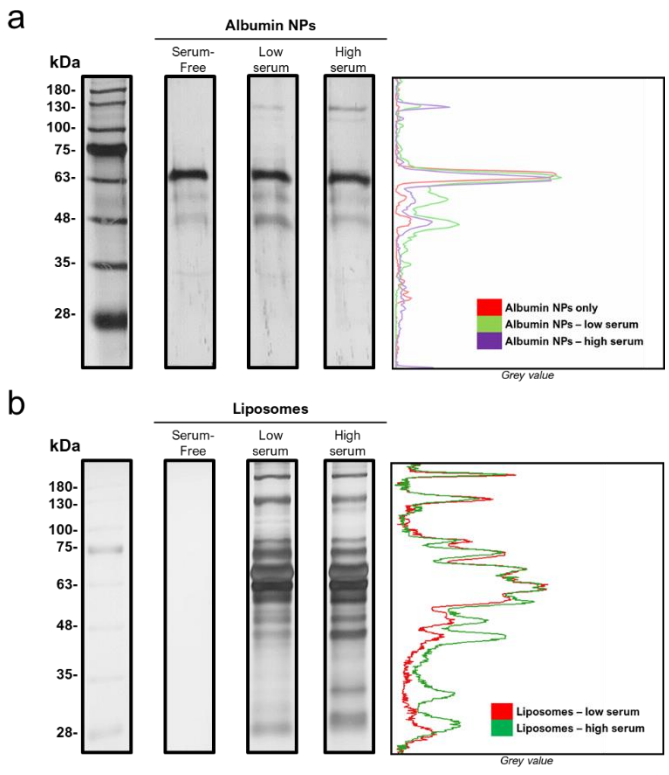

Figure 1. Identification of hard corona proteins on albumin NPs and liposomes on SDS-PAGE electrophoresis along with densitometry analysis of each band.

Around 125 proteins were found in the corona of albumin NPs and 316 proteins in the corona of the liposomes (**Supplementary Tables S1-S4**). We then classified some of the main proteins which were identified by LC-MS/MS based on normalized spectral count. Normalization was used to semi-quantitatively assess the amount of every protein elucidated from the total protein corona and to define the contribution of each protein in its correlation with protein corona formation[22].

Fig. 2 shows the classification of proteins within the corona of each NP type based on the protein's isoelectric point (pI) and molecular weight (MW). The majority of proteins recruited to the corona of each type of NP had a low pI (**Fig. 2(c)**), specifically a pI of 5 to 6 (**Fig. 2(a)**), independent of whether it was incubated in a low or high concentration of serum. Interestingly, some proteins with a lower pI were recruited to the surface of liposomes in greater amounts than to the surface of albumin NPs at both serum concentrations. The cationic surface intensity was enriched with proteins with a pI < 7, while a typical anionic surface would attract more proteins with a pI > 7. This result is in good agreement with a previous study which showed that the cationic charge of NPs adsorbs more proteins with pI < 5.5, and anionic NPs are more likely to attract proteins with a pI > 5.5[44].

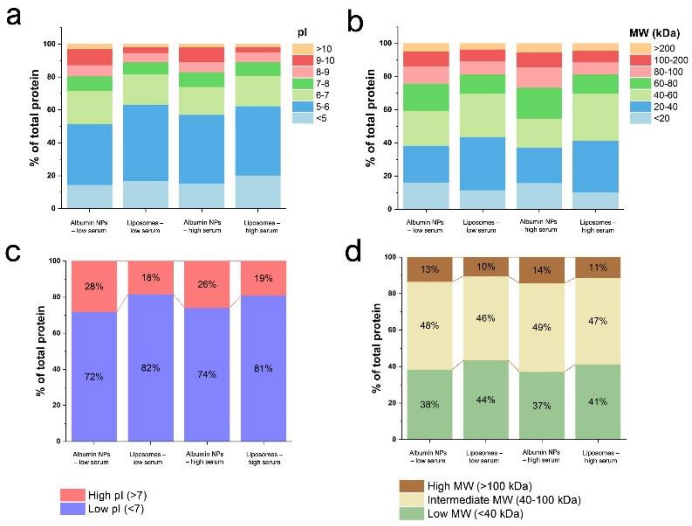

Figure 2. Classification of hard corona proteins identified from albumin NPs and liposomes after low and high serum incubations based on the (a) isoelectric point and (b) molecular weight (kDa). The summarized patterns of (c) isoelectric point and (d) molecular weight of hard corona proteins identified from albumin NPs and liposomes.

Further, it was observed that both NPs mainly recruited proteins with MWs between 20 and 80 kDa (**Fig. 2(b), (d)**). In addition, proteins with an MW > 60 kDa were found in slightly greater amounts in the corona of albumin NPs compared to liposomes. This result further suggests that albumin NPs might attract rather similar MW proteins, such as serum albumin as well, at different serum concentrations.

Among the most recognizable proteins, it was shown in heatmaps that complement proteins were the most abundant on the surface of liposomes with both low and high serum incubations. In contrast, apolipoproteins were the most common proteins present on albumin NP surfaces (**Fig. 3** and **Supplementary Tables S1-S4**). Further, the five most common proteins found in the corona of each NP type were sorted to observe which corona proteins were typically recruited to each NP (**Supplementary Fig. S3**).

Apolipoprotein C-IV and hemoglobin sub-unit alpha were identified in the albumin NPs, but were absent or less often found among proteins on liposomes. The same evidences are in accordance with the previous findings from other reports[45, 46]. The protein composition of the hard corona bound to the two different NPs greatly differed, even though the two types of NPs were exposed to the same serum concentrations[47, 48]. These results suggested that different surface features (physicochemical properties) of each NP type and the complexity of the biological fluids enriched specific protein corona compositions and abundances[49-54]. For example, complement C3 appeared to be the most abundant on the interface of liposomes due to the larger number of hydrophobic residues on its surface than other proteins.

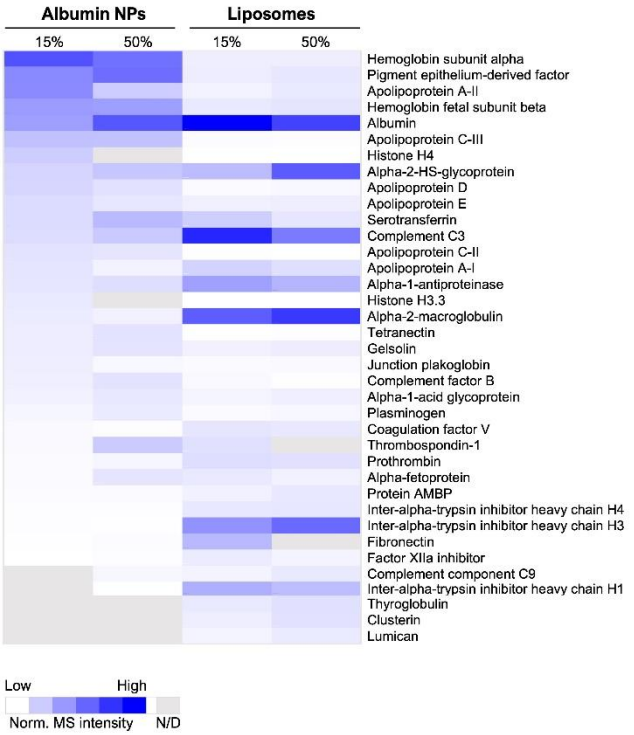

Figure 3. Heatmaps of protein corona sorted based on normalized spectra counts obtained from LC-MS/MS for albumin NPs and liposomes upon incubation with low and high serums. N/D, not detected.

Some proteins identified as being present at high concentrations in the hard corona of albumin NPs appear to be rare among coronas found on other NPs types[55, 56]. This indicates that different serum concentration could result in different total amounts of protein present in the environment of the NPs and also different kinds of protein recruited to the surface of the albumin NPs and liposomes.

Isothermal titration calorimetry (ITC)

The adsorption process and binding affinity of each NP with serum were investigated through ITC measurements. ITC directly measures the heat change of binding occurrence from two different solutions by injecting the first solution (titrant) into the second one (titrate)[57]. In every injection process, an equilibrium between the two is established causing heat to be absorbed or released. Herein, a low serum concentration was titrated into albumin NPs and liposomes. Both NPs had similar particle numbers against the titrated serum thus, obtaining directly comparable results. The change in heat during titration was observed and recorded, while K_a, ΔH, and n were obtained by curve fitting analyses using an independent binding model. Interactions between the serum and albumin NPs or liposomes were indicated to be exothermic as they demonstrated a typical negative value of the change in enthalpy ($\Delta H < 0$) as heat is being released during the titration process (as shown in **Table 2**, **Supplementary Fig. S4**). Changes in enthalpy for albumin NPs (-109 ± 38.80 kJ mol^{-1}) and liposomes (-94 ± 12.37 kJ mol^{-1}) suggested that spontaneous isothermal binding occurred.

The molar concentration of serum was defined according to that of BSA (MW= 66.4 kDa) and adjusted to molar values. We considered the BSA molar value in this regard due to its abundance in the serum (comprising 90% of albumin)[58]. As shown in **Table 2**, the K_a of serum binding to albumin NPs was significantly less than that for liposomes, indicating less exothermal behavior as presented by lower binding affinity. Further, the stoichiometric ratio obtained from the independent binding analysis indicated the total number of protein molecules that interacted with one particle of albumin NPs or liposomes. It significantly showed that either due to its intrinsic or physicochemical factors, a single albumin NP and a liposome strongly attracted approximately 18 and 76 serum proteins, respectively.

Table 2. Thermodynamic parameters of albumin nanoparticles (NPs) and liposomes in interaction with fetal bovine serum upon fitting with an independent model.

	K_a (10^4) M^{-1}	n	ΔH (kJ mol^{-1})	ΔS (kJ mol^{-1} K^{-1})
Albumin NPs	118.7 ± 64.49	14.8 ± 2.76	-109 ± 38.80	-250.1 ± 134.18
Liposomes	302.9 ± 190.14	73.9 ± 7.28	-94 ± 12.37	-195.6 ± 39.50

A smaller number of serum proteins were detected on albumin NPs, which indicated that fewer proteins were recruited to their surface and they contacted fewer free proteins (referred to as soft-corona protein) than did liposomes. These binding results are in accordance with those observed in the LC-MS/MS results, in which more proteins were found on the surface of liposomes than on albumin NPs. The distinct properties between the two NPs underline the above results.

View Article Online
DOI: 10.1039/D3NR04862D

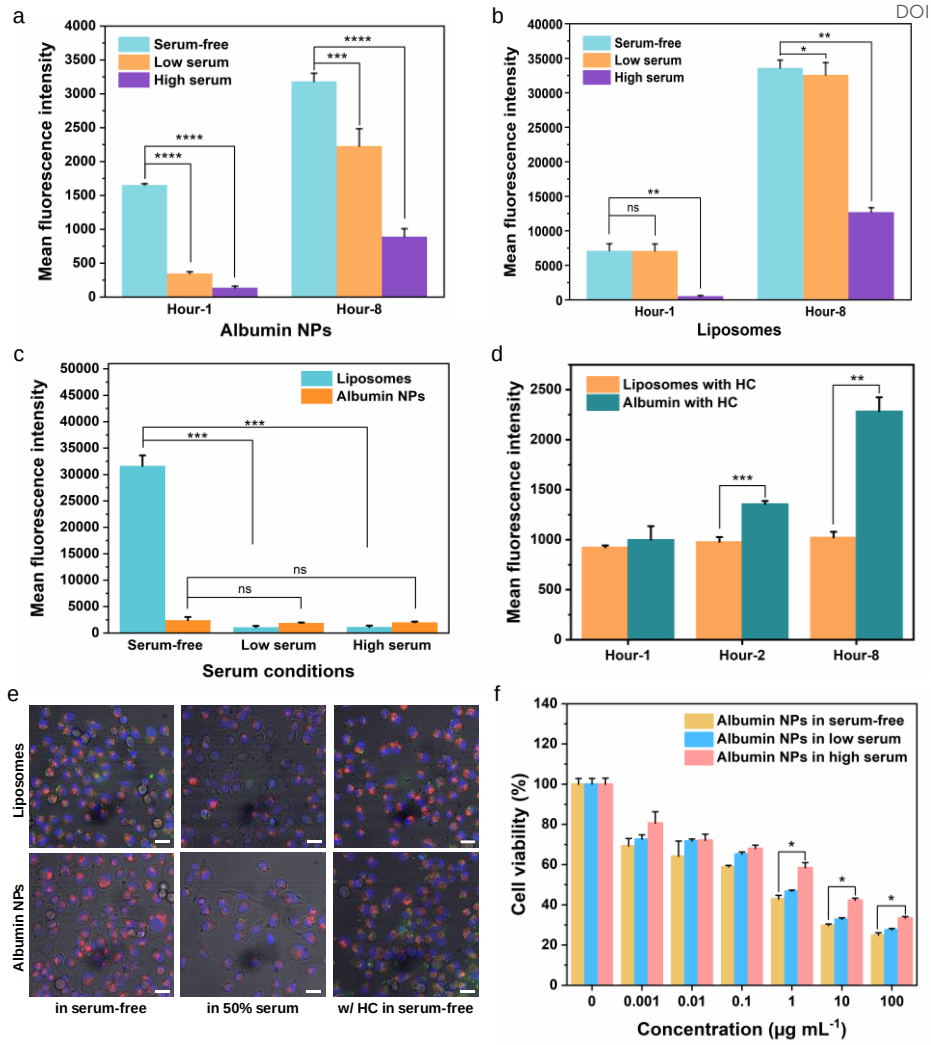

Figure 4. (a) Albumin NPs and (b) liposomes uptakes by MIA PaCa-2 cells in serum-free, low, and high-incubated serum media upon 1- and 8-hour incubations. (c) Both nanoparticles uptakes by Raw 264.7 cells in serum-free, low, and high-incubated serum media upon 30 min incubation. (d) The flow cytometry data obtained for nanoparticles in complex with HC for each type of nanoparticles. (e) Confocal images of both nanoparticles internalizations in MIA PaCa-2 cells upon 1 h incubation in serum-free media, media containing 50% serum, and with protein corona complex (HC = hard corona) in serum-free media. The colors in the merged images refer to both nanoparticles (green), lysosome (red), and nuclei (blue). Scale bar = 25 μm. (f) Cell viability assay of drugs-albumin NPs on MIA PaCa-2 cells in different serum concentrations. All bars were presented as means ± standard deviations (s.d.) for three experimental replicates ($n = 3$); significance level compared with cells incubated with liposomes in serum-free only is indicated in Figure 4c (*$p \leq 0.05$, **$p \leq 0.01$, ***$p \leq 0.001$, ****$p \leq 0.0001$, *Student's t test*).

Specifically, the liposomes are positively charged and thus attracted more proteins than did albumin NPs. Nevertheless, other factors affecting the binding affinity are always present and play a role during the calorimetry titration, including the enthalpy contributed by the surrounding environment. This also reflects the presence of noncovalent interaction that takes place during such interactions, for instance, hydrogen bonds, dipole-dipole interactions, and hydrophobic effects, which form as a result of interactions between serum proteins and NP surfaces[57].

Cellular uptake affected by the serum concentration

To evaluate the influence of serum on the uptake of NPs by cells, experiments were conducted with similar serum concentrations as were previously used to incubate albumin NPs and liposomes. For the cellular study, a fluorescent dye (i.e., DiO) was incorporated into both NPs during synthesis. Since each NP was prepared in a different way, the ratio of encapsulated DiO differed. Therefore, we used the same number of particles in the cell studies for both types of NPs while keeping the same final concentration of DiO. Both NPs showed time-dependent profiles with an increase in the mean fluorescence intensity in MIA PaCa-2 tumor cells (**Fig. 4(a-b)**). In a low serum concentration, the uptake of liposomes was fairly similar to those found in a serum-free condition at both incubation times. The reduced uptake of liposomes was further indicated in a high serum condition.

Meanwhile, the uptake of the albumin NPs showed the same order at both incubation times (serum-free > low concentration > high concentration). This suggests that in biological conditions, the

presence of a higher or lower serum concentration or any state of biological milieu could dramatically change NP uptake by cells, which is typically important for the purpose of studying specific diseases. For instance, serum conditions in patients with diabetes or cancer differ from each other[59, 60].

The selection of 15% and 50% serum concentrations in our study aimed to represent low and high serum concentrations introduced to the cells and to investigate the impact of serum concentration on protein content, protein corona formation, and cellular uptake of the nanoparticles. Furthermore, these concentrations were used as models to understand the relationship between serum concentration conditions during disease treatment, as indicated in the MTT studies on cell cytotoxicity. In addition, other research groups had also reported the use of serum in a range of 0.1% to 8% [61] and 1% to 100% [22, 62-64] to study the effect of serum on NPs.

It is well known that any substances introduced into the bloodstream can encounter a condition wherein the protein corona interacts with them. This state likely triggers opsonization by the mononuclear phagocytic system (MPS), typically due to recognition by macrophages [65]. Albumin NPs and liposomes were introduced into the RAW 264.7 macrophage cells following three different conditions of no serum, high-concentration serum, and low-concentration serum. In macrophages cells, we observed that the uptake patterns of liposomes and albumin NPs differed compared to those in cancerous cells. It was obvious that liposomes showed the highest uptake by macrophages in serum-free media (**Fig. 4(c)**). The glycosylated outer leaflet of the plasma membrane is known to possess a negative charge potential[66]. Thus, this large uptake was likely a result of attractive electrostatic interactions between cationic liposomes and anionic plasma membrane. In the presence of serum, the uptake of liposome was significantly suppressed. The effect of this serum is different compared to the condition of cancer cells, where the serum around macrophages inhibits cell uptake more profoundly than the two NPs uptake by the cancer cells.

Meanwhile, albumin NPs uptake by macrophages was likely to be unchanged from the effect of the presence of serum. Even though there was a slight decrease compared to those incubated in serum-free media, it was not as significant as the effect of serum on the uptake of liposomes which was due to nonspecific electrostatic interactions (**Fig. 4(c)**). As it is known that macrophages have multiple ways of internalizing pathogens and foreign entities, it is possible that the uptake of liposomes and albumin NPs occurs *via* different mechanisms.

The internalization of NPs by the cells was further evaluated through confocal microscopy. A difference in the uptake of NPs by cells with a hard corona of proteins was seen compared to bare NPs (**Fig. 4(d-e)**). The hard corona present on the NPs was obtained following a separation process according to the protein corona preparation method. Since, in direct serum incubation, there is no process to separate the proteins in the corona of the NPs from free and unbound proteins, interactions of the NPs with cells were likely blocked by the presence of abundant free protein in the serum resulting in lower uptake during the incubation period (as presented in **Supplementary Figs. S5-S6**). Interestingly, the presence of the hard protein corona on albumin NPs allowed greater amounts of NPs than liposomes to be engulfed by the cancer cells at the measured time points (**Fig. 4(e)**). This indicated that the hard corona protein could increase the internalization of Albumin NPs in comparison to liposomes.

To distinguish the influence of the presence of serum on the pharmacological state, we employed an active pharmaceutical compound previously reported (called MPT0B291) to be incorporated into the albumin NPs (MPT0B291/albumin NPs)[18, 23]. Herein, a range of MPT0B291 concentrations in albumin NPs was incubated with MIA PaCa-2 cells for 24 h. With an increase in the dose of MPT0B291/albumin NPs, the cell cytotoxicity in MIA PaCa-2 cells also increased (**Fig. 4(f)**). Similarly, cell viability data showed that cytotoxicity decreased as the concentration of serum increased. The presence of serum in this regard seemed to influence the drug/particle uptake by MIA PaCa-2 cells, compared to a free-serum condition. In the absence of serum, the resulting cytotoxicity effect on cells was significantly higher, while in contrast to those incubated with certain serum concentrations, the cytotoxicity was lower. Further, the 50% inhibitory concentration (IC_{50}) value after incubation of 24 h in different serum conditions were determined as 0.6179 ± 0.0447, 0.7354 ± 0.3466, and 3.2700 ± 0.5428 μg/mL for serum-free, low, and high serum concentrations, respectively (**Supplementary Table S5**). The observed increase in the IC_{50} dose signified a reduction in the antiproliferative activity of MPT0B291 (the active compound) with the gradual increase of serum concentration. These outcomes underline that the presence of serum interferes with the NPs being internalized by the cancer cells, leading to a decrease in the antitumor effects.

Albumin receptors, such as glycoprotein 60 or glycoprotein 30, are highly present on particular cancer cells. These receptors are the primary route through which albumin NPs are internalized, which then triggers caveolar endocytosis[67]. This receptor is known to internalize albumin for further catabolism, which induces no immune signal. Meanwhile, liposomes demonstrated different uptake mechanisms in the three different concentrations of serum. In serum-free media, the large amount of uptake of liposomes was largely a result of direct electrostatic interactions with cell membranes. In the presence of serum, the amount of uptake of liposomes was reduced to a similar level as was seen with albumin NPs. Interestingly, liposomes in a hard corona complex showed less uptake than those present in serum-free media. The liposome-hard corona complex seemed to be internalized *via* caveolae-mediated endocytosis which was similar to the mechanism by which albumin NPs were internalized, and this route is known in fact to be used by negatively charged or neutral entities[68, 69]. As shown by LC-MS/MS results, the most prevalent proteins on liposomes belonged to the opsonin type, which are known to be the most recognized by the immune system. Therefore, in the presence of most of these proteins, recognition by the corresponding cancer cells would be possible through any natural receptor or *via* passive uptake permitting several ways for the NPs to be engulfed by the cells, as complement receptors would only be highly expressed by antigen presenting cells or other immune cells (*via* phagocytosis)[70]. The role of protein serum is summarized in **Scheme 1**.

View Article Online
DOI: 10.1039/D3NR04862D

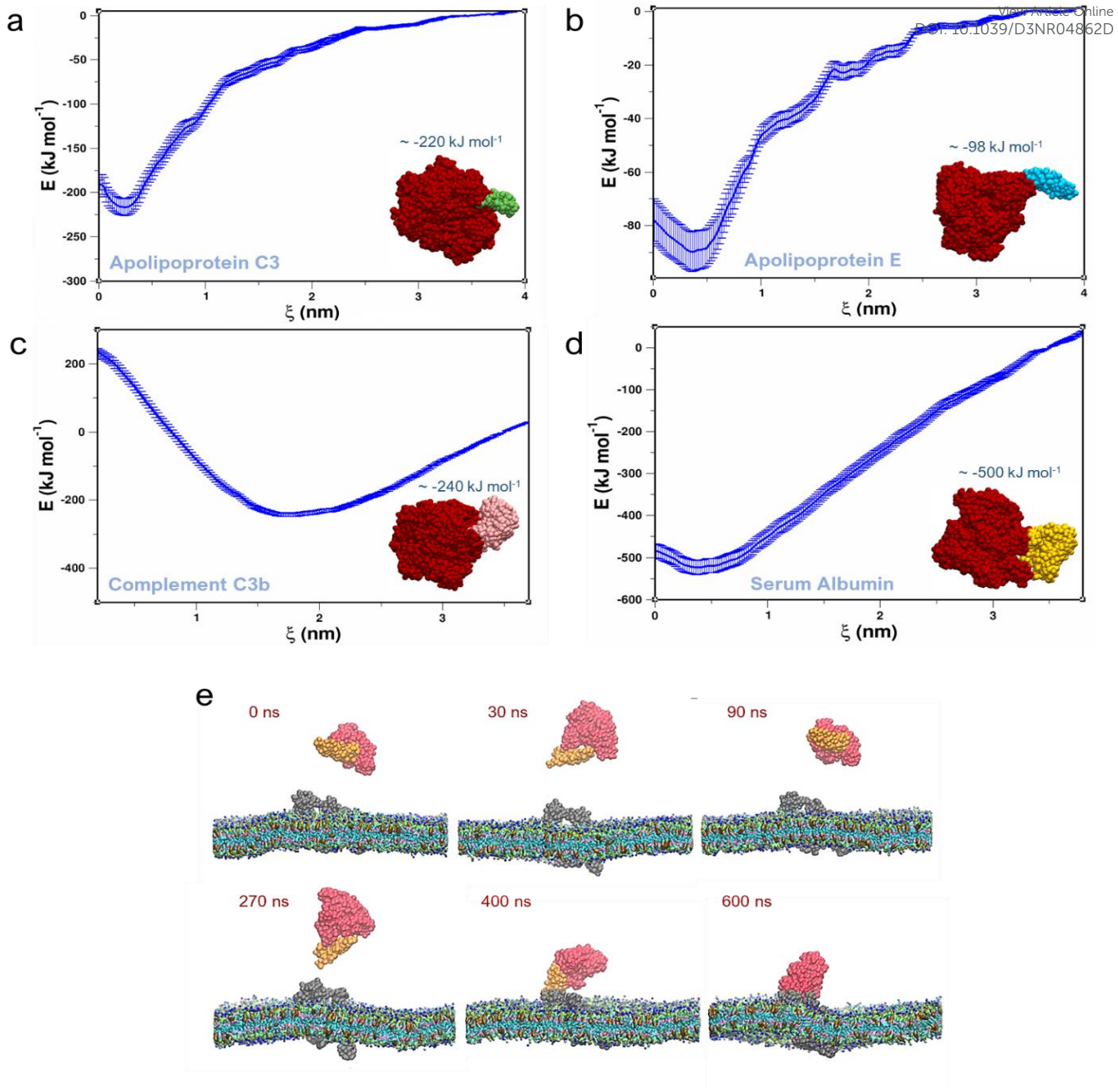

Figure 5. Thermodynamics profile obtained from potential mean force through umbrella sampling simulation for each protein (depicted in different colors: (a) apolipoprotein C3 (green), (b) apolipoprotein E (blue), (c) complement C3b (mauve), and (d) albumin (yellow)) toward the albumin NPs (depicted in red color). (e) Snapshot of molecular dynamics simulation of albumin NPs (represented by subset of an albumin protein) with apolipoprotein E toward the membrane bilayer in the presence of LDL-R protein.

Coarse-grained molecular dynamics on albumin NPs

We further intended to describe how albumin NPs behave toward proteins that were identified in their corona through LC-MS/MS studies. Herein, molecular dynamics simulations were performed on an albumin NP to provide a detailed description of the various types of interactions used by proteins in the corona to bind to particle surface/membrane. To do so, free energy binding through umbrella sampling simulation was conducted. Interaction kinetics of several proteins which were abundantly found on NP surface were evaluated by sampling binding events between protein and the interface of an albumin NP. Simulations were initiated by a coarse-grained construction of an albumin NP by incorporating five HSA protein units into a complex with beads according to atom-to-atom information. All biomolecular beads were relaxed through optimization and thus slowly equilibrated stage-by-stage; the periodic boundary system reached an equilibration condition before the MD simulation.

The next conformation of the complex was taken from the final timestep of these initial simulations and then used as the

View Article Online
DOI: 10.1039/D3NR04862D

starting confirmation for umbrella sampling simulation which were used to calculate the potential of the mean force (PMF; kJ mol^{-1}; rather similar to ΔG values). From umbrella sampling simulations, the binding modulation of each complex was averaged over the simulation time and possible binding events (**Fig. 5(a-d)**). Results showed that all of the proteins induced spontaneous interactions with albumin NP. Among the four proteins investigated, serum albumin had the highest PMF value due to its greater exposed surface area which could interact with albumin NP (ca. -500 kJ mol^{-1}). analysis, such that serum albumin had the smallest PMF and therefore had the most energetically favorable interaction with NP and was the most prevalent protein in the hard corona. In contrast, apolipoprotein E had the largest PMF, which indicated that it was the least energetically favorable of the four proteins and it also was the least prevalent protein in the hard corona.

To ensure the reliability of our results, two additional simulations were performed that confirmed the convergence of the potential of mean force (PMF) profiles in both figures. Notably, the PMF profiles from these additional simulations

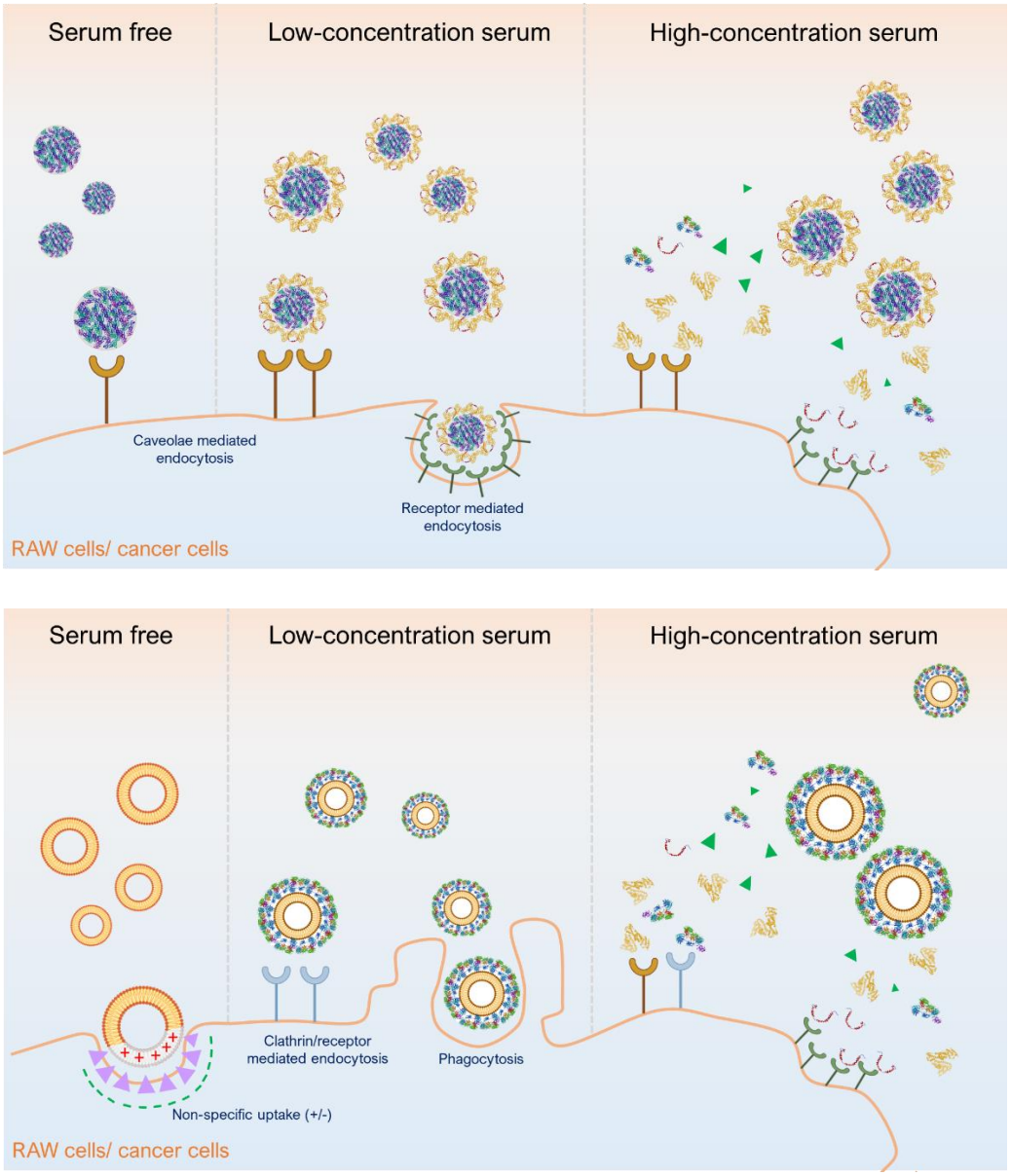

Scheme 1. Schematic overview of albumin NPs (top) and liposomes (bottom) uptakes by the cells.

Apart from being larger, complement C3b protein interacted with the outer interface of NP residues and had a lower PMF value than serum albumin and a similar value as apolipoprotein C3 (ca. -220 kJ mol^{-1}). Meanwhile, PMF values of different proteins were consistent with the propensity of each within the hard corona as determined by the LC-MS/MS showed no significant changes compared to the original simulations. Hence, the ΔG trends of the systems were comparable with the experimental findings. The PMF results characterized thermodynamic parameters down to the molecular level involving the physicochemical properties of proteins with less dependence on protein size. Electrostatic

interactions and hydrophobic effects generally play key roles considering that the interface of the albumin NPs also had a slightly higher number of hydrophobic residues, which facilitated more possible contacts with proteins in the hard corona.

A subset of the previously obtained NP-protein corona complex (i.e., albumin or apolipoprotein E) were used in further simulations to evaluate their interactions with the membrane model. The membrane model used was a bilayer lipid which had a specific composition similar to that of a tumor membrane[28]. The protein complex was then simulated towards the lipid membrane under two different conditions: in the presence or absence of specific cell receptors.

We proposed the LDL-R for use here because it is recognized as an important receptor for LDL and several mechanisms related to its role in lipid metabolism and other cellular biological processes have been studied, including being highly expressed in MIA PaCa-2 and macrophage cells[71].

As to results, a typical interaction was indicated in the protein complex with the albumin corona which allowed interactions with the membrane region *via* hydrophobic interactions. In contrast, the NP with the apolipoprotein E corona had an increased center-of-mass distance due to apolipoprotein E in the complex moving away from the membrane after a dynamic period of 60 ns (**Supplementary Figs. S7-S8**).

Since the apolipoproteins were abundantly found on albumin NPs as hard corona proteins and to represent apolipoprotein uptake, we simulated the molecular mechanism by the LDL-R present in the membrane. The LDL-R is known as the receptor that controls cholesterol distribution in mammalian cells. It regulates a wide range of lipoproteins from the circulation through receptor-mediated endocytosis which is further internalized by cells[72, 73]. The extracellular domain of LDL-R is rich with cysteine-residues (localized on R1 to R7 repeat units) and reported to act in recognizing apolipoprotein moieties and as ligand-binding sites[74]. The external negative charge counterpart present allows it to interact with positively charged residues of apolipoproteins[75].

The subset of the NP-apolipoprotein E complex initially hovered at an equal distance as in the previous run from the receptor-containing membrane. Adequate equilibration was then followed by an intensive production step of molecular dynamics simulation. After 200 ns, the complex moved closer to the bilayer membrane where cysteine-rich LDL-R residues were exposed, and then the distance between the complex and the bilayer membrane was gradually reduced (**Fig. 5(e)**). After 600 ns was reached, apolipoprotein E drew in albumin to the membrane region possibly mediated by its interaction with LDL-R. Meanwhile, when compared with **Supplementary Fig. S8**, the protein complexes appeared to move away from the membrane bilayer as the simulation time increased. When a specific receptor is present on the cellular membrane, it outperforms the recognition of the appropriate ligand/protein and simultaneously initiates membrane binding and further processes within the cell.

Overall, the simulations demonstrated that corona protein present on the NP potentially regulated protein interactions on the NP surface which drove the NP to a specific internalization pathway or to be taken up through different mechanisms. The dynamic simulation of LDL-R and protein interactions further emphasized the LDL-R's function as a gate for the endocytosis pathway, wherein NP bound to apolipoproteins on its surface (NP-apolipoprotein) might undergo a similar internalization process driven by the presence of hard corona proteins to reach its receptor in a such biologically complex condition[74, 75]. In other words, NPs-apolipoproteins might bind to the LDL-R on cell surface and create a complex which would then be internalized by the cell[76].

Since cancerous cells are rich in permeable tumor neo-vessels, it is then suggested that more of the LDL-R would be localized on this site than on normal cells. As a consequence, apolipoproteins would be highly present, and thereby would be a chance for NPs-apolipoproteins to be highly internalized by the cancer cells. Since not all the cell types possess LDL-R on their cell surface, the interaction mechanism could possibly take place through another receptor type or other mechanism, such as LOX-1 receptor on A549 cells (i.e., lung cancer cell line)[77]. However, a similar modelling approach might be applied for the study of interactions between corona proteins and selected receptors.

Conclusion

Albumin NPs and liposomes have been characterized solely in terms of protein corona identification, formation, and the composition. It was found that two different NPs (albumin NPs and liposomes) developed different protein corona profiles. The neutral or rather slightly negatively charged albumin NPs were capable of encountering protein corona involvement rather than the positively charged PEGylated liposomes. The protein corona of the NPs highly depends on the entities and components of the surrounding serum or biological fluid. Based on these results, unbound proteins hindered the internalization of the NPs into the cells as implied by the increase in the serum concentration. The hard protein corona seemed to drive greater internalization of the NPs into the MIA PaCa-2 cells compared to those with the presence of a soft protein corona. On the other hand, different serum concentrations indeed affected the NPs uptake by the cells. In such a way, it is suggested to consider the use of rather-similar contents of serum as implying a closer condition toward the state of a studied disease.

A computational study encompassed a molecular dynamics simulation to elucidate the process beyond biological interactions of NP with the protein corona, and *vice versa*. The binding free energy from the simulation results supported the findings from abundance sequences on protein serum found in proteomics. Further, the results showed that the presence of the receptor on the lipid bilayer was highly attracted to its corresponding target, apolipoprotein E, which was bound to albumin NP. Since cancerous cells are rich in permeable tumor neo-vessels, it is thus estimated that more interactions between

LDL-R and apolipoproteins would take place, which indicates that if shielding of the NPs with apolipoproteins, such as the dysopsonin protein, is performed, it would potentially greatly improve the uptake of NPs by the cells through this route in the actual biological conditions.

Author Contributions

A.D.P: Investigation; Methodology; Writing - original draft; Validation; Visualization. **M.-J.H**: Supervision; Methodology; Validation; Resources. **C.-L.H**: Supervision; Methodology; Resources; Data curation. **F.-C.C**: Writing - review & editing. **C.-H.H**: Data curation; Resources. **C.D.L**: Supervision; Data curation; Writing - review & editing. **C.-M.H**: Supervision; Resources; Validation; Writing - review & editing.

Conflicts of interest

The authors declare no conflict of interest.

Acknowledgements

This work was financially supported by grant from the Ministry of Science and Technology (MOST109-2221-E-038-001-MY3 and MOST110-2113-M038-001-MY3) and National Science and Technology Council (NSTC112-2221-E-038-014), Taiwan. Mass spectrometry data were acquired at the Common Mass Spectrometry Facilities located at the Department of Chemistry, National Taiwan University (Taiwan). The authors thank Dr. Bayu Tri Murti (Semarang College of Pharmaceutical Sciences (STIFAR) Semarang, Indonesia). The assistance of Dr. Pu-Sheng Wei (Taipei Medical University) in confocal imaging measurements is greatly acknowledged. The authors gratefully thank Core Facility of Taipei Medical University for facilitating the instrumental uses. The authors also thank The National Center for High-Performance Computing, Hsinchu City, Taiwan for providing the necessary computational resources

Notes and references

‡ Additional figures, tables, and method related to this work are available as **Supplementary Information** in separated files.

1. M. Mahmoudi, N. Bertrand, H. Zope and O. C. Farokhzad, *Nano Today*, 2016, **11**, 817-832.
2. J. Wagner, M. Dillenburger, J. Simon, J. Oberländer, K. Landfester, V. Mailänder, D. Y. W. Ng, K. Müllen and T. Weil, *Chem. Commun.*, 2020, **56**, 8663-8666.
3. E. Quagliarini, L. Digiacomo, S. Renzi, D. Pozzi and G. Caracciolo, *Nano Today*, 2022, **47**, 101657.
4. J.-M. Rabanel, J. Faivre, C. Zaouter, S. A. Patten, X. Banquy and C. Ramassamy, *Biomaterials*, 2021, **277**, 121085.
5. R. Madathiparambil Visalakshan, L. E. González García, M. R. Benzigar, A. Ghazaryan, J. Simon, A. Mierczynska-Vasilev, T. D. Michl, A. Vinu, V. Mailänder, S. Morsbach, K. Landfester and K. Vasilev, *Small*, 2020, **16**, 2000285.
6. N. Desai, V. Trieu, B. Damascelli and P. Soon-Shiong, *Transl. Oncol.*, 2006, DOI: 10.1593/tlo.09109, 59-64.
7. M. M. El-Hammadi and J. L. Arias, *Expert Opin. Ther. Pat.*, 2019, **29**, 891-907.
8. A. Jain, S. K. Singh, S. K. Arya, S. C. Kundu and S. Kapoor, *ACS Biomater. Sci. Eng.*, 2018, **4**, 3939-3961.
9. J. S. Suk, Q. Xu, N. Kim, J. Hanes and L. M. Ensign, *Adv. Drug Deliv. Rev.*, 2016, **99**, 28-51.
10. A. Gabizon, H. Shmeeda and Y. Barenholz, *Clin. Pharmacokinet.*, 2003, **42**, 419-436.
11. T. Shimizu, T. Ishida and H. Kiwada, *Immunobiology*, 2013, **218**, 725-732.
12. J. T. Huckaby, T. M. Jacobs, Z. Li, R. J. Perna, A. Wang, N. I. Nicely and S. K. Lai, *Commun. Chem.*, 2020, **3**, 1-8.
13. N. d'Avanzo, C. Celia, A. Barone, M. Carafa, L. Di Marzio, H. A. Santos and M. Fresta, *Adv. Ther.*, 2020, **3**, 1900170.
14. J. Simon, L. K. Müller, M. Kokkinopoulou, I. Lieberwirth, S. Morsbach, K. Landfester and V. Mailänder, *Nanoscale*, 2018, **10**, 10731-10739.
15. F. Giulimondi, L. Digiacomo, D. Pozzi, S. Palchetti, E. Vulpis, A. L. Capriotti, R. Z. Chiozzi, A. Laganà, H. Amenitsch, L. Masuelli, G. Peruzzi, M. Mahmoudi, I. Screpanti, A. Zingoni and G. Caracciolo, *Nat. Commun.*, 2019, **10**, 3686.
16. H. Kim, D. Röth, Y. Isoe, K. Hayashi, C. Mochizuki, M. Kalkum and M. Nakamura, *Colloids Surf. B*, 2021, **199**, 111527.
17. X. Hou, T. Zaks, R. Langer and Y. Dong, *Nat. Rev.*, 2021, **6**, 1078-1094.
18. A. D. Putri, P.-S. Chen, Y.-L. Su, J.-P. Lin, J.-P. Liou and C.-M. Hsieh, *Pharmaceutics*, 2021, **13**, 1728.
19. W. Deng, W. Chen, S. Clement, A. Guller, Z. Zhao, A. Engel and E. M. Goldys, *Nat. Commun.*, 2018, **9**, 2713.
20. C.-L. Han, C.-W. Chien, W.-C. Chen, Y.-R. Chen, C.-P. Wu, H. Li and Y.-J. Chen, *Mol. Cell Proteomics*, 2008, **7**, 1983-1997.
21. J. Cox and M. Mann, *Nat. Biotechnol.*, 2008, **26**, 1367-1372.
22. M. P. Monopoli, D. Walczyk, A. Campbell, G. Elia, I. Lynch, F. Baldelli Bombelli and K. A. Dawson, *J. Am. Chem. Soc.*, 2011, **133**, 2525-2534.
23. B. Buyandelger, E. E. Bar, K. S. Hung, R. M. Chen, Y. H. Chiang, J. P. Liou, H. M. Huang and J. Y. Wang, *Int. J. Biol. Sci.*, 2020, **16**, 3184-3199.
24. E. Lindahl, M. J. Abraham, B. Hess and D. van der Spoel, GROMACS 2019 Manual (Version 2019), https://doi.org/10.5281/zenodo.2424486, DOI: 10.5281/zenodo.2424486).
25. S. J. Marrink, H. J. Risselada, S. Yefimov, D. P. Tieleman and A. H. de Vries, *J. Phys. Chem. B*, 2007, **111**, 7812-7824.
26. L. Monticelli, S. K. Kandasamy, X. Periole, R. G. Larson, D. P. Tieleman and S.-J. Marrink, *J. Chem. Theory Comput.*, 2008, **4**, 819-834.
27. X. Periole, M. Cavalli, S.-J. Marrink and M. A. Ceruso, *J. Chem. Theory Comput.*, 2009, **5**, 2531-2543.
28. T. Rivel, C. Ramseyer and S. Yesylevskyy, *Sci. Rep.*, 2019, **9**, 5627.
29. H. Berendsen, J. Postma, W. van Gunsteren, A. DiNola and J. Haak, *J. Chem. Phys.*, 1984, **81**, 3684-3690.
30. K. Giri, K. Shameer, M. T. Zimmermann, S. Saha, P. K. Chakraborty, A. Sharma, R. R. Arvizo, B. J. Madden, D. J. Mccormick and J.-P. A. Kocher, *Bioconjug. Chem.*, 2014, **25**, 1078-1090.

31. D. Pozzi, G. Caracciolo, L. Digiacomo, V. Colapicchioni, S. Palchetti, A. L. Capriotti, C. Cavaliere, R. Zenezini Chiozzi, A. Puglisi and A. Laganà, *Nanoscale*, 2015, **7**, 13958-13966.
32. R. Rampado, S. Crotti, P. Caliceti, S. Pucciarelli and M. Agostini, *Front. Bioeng. Biotechnol.*, 2020, **8**, 166-166.
33. L. Digiacomo, F. Giulimondi, A. L. Capriotti, S. Piovesana, C. M. Montone, R. Z. Chiozzi, A. Laganà, M. Mahmoudi, D. Pozzi and G. Caracciolo, *Nanoscale Advances*, 2021, **3**, 3824-3834.
34. P. S. R. Naidu, M. Norret, N. M. Smith, S. A. Dunlop, N. L. Taylor, M. Fitzgerald and K. S. Iyer, *Langmuir*, 2017, **33**, 12926-12933.
35. N. Onishchenko, D. Tretiakova and E. Vodovozova, *Acta Biomaterialia*, 2021, **134**, 57-78.
36. M. Lundqvist, J. Stigler, G. Elia, I. Lynch, T. Cedervall and K. A. Dawson, *PNAS*, 2008, **105**, 14265-14270.
37. D. Pozzi, V. Colapicchioni, G. Caracciolo, S. Piovesana, A. L. Capriotti, S. Palchetti, S. De Grossi, A. Riccioli, H. Amenitsch and A. Laganà, *Nanoscale*, 2014, **6**, 2782-2792.
38. M. Debayle, E. Balloul, F. Dembele, X. Xu, M. Hanafi, F. Ribot, C. Monzel, M. Coppey, A. Fragola, M. Dahan, T. Pons and N. Lequeux, *Biomaterials*, 2019, **219**, 119357.
39. K. A. Majorek, P. J. Porebski, A. Dayal, M. D. Zimmerman, K. Jablonska, A. J. Stewart, M. Chruszcz and W. Minor, *Mol. Immunol.*, 2012, **52**, 174-182.
40. K. Yamada, K. Yokomaku, M. Kureishi, M. Akiyama, K. Kihira and T. Komatsu, *Sci. Rep.*, 2016, **6**, 1-11.
41. A. Bujacz, *Acta Crystallogr. D*, 2012, **68**, 1278-1289.
42. D. Agudelo, P. Bourassa, J. Bruneau, G. Berube, E. Asselin and H.-A. Tajmir-Riahi, *PLOS ONE*, 2012, DOI: 10.1371/journal.pone.0043814.
43. P. Kandagal, S. Ashoka, J. Seetharamappa, S. Shaikh, Y. Jadegoud and O. B. Ijare, *J. Pharm. Biomed. Anal.*, 2006, **41**, 393-399.
44. L. Abarca-Cabrera, P. Fraga-García and S. Berensmeier, *Biomaterials Research*, 2021, **25**, 12.
45. A. Salvati, A. S. Pitek, M. P. Monopoli, K. Prapainop, F. B. Bombelli, D. R. Hristov, P. M. Kelly, C. Åberg, E. Mahon and K. A. Dawson, *Nature Nanotechnology*, 2013, **8**, 137-143.
46. Y.-F. Wang, C. Zhang, K. Yang, Y. Wang, S. Shan, Y. Yan, K. A. Dawson, C. Wang and X.-J. Liang, *National Science Review*, 2021, **8**.
47. Y. Yan, K. T. Gause, M. M. J. Kamphuis, C.-S. Ang, N. M. O'Brien-Simpson, J. C. Lenzo, E. C. Reynolds, E. C. Nice and F. Caruso, *ACS Nano*, 2013, **7**, 10960-10970.
48. A. Lesniak, F. Fenaroli, M. P. Monopoli, C. Åberg, K. A. Dawson and A. Salvati, *ACS Nano*, 2012, **6**, 5845-5857.
49. R. Eigenheer, E. R. Castellanos, M. Y. Nakamoto, K. T. Gerner, A. M. Lampe and K. E. Wheeler, *Environmental Science: Nano*, 2014, **1**, 238-247.
50. N. Liu, M. Tang and J. Ding, *Chemosphere*, 2020, **245**, 125624.
51. H. Mohammad-Beigi, Y. Hayashi, C. M. Zeuthen, H. Eskandari, C. Scavenius, K. Juul-Madsen, T. Vorup-Jensen, J. J. Enghild and D. S. Sutherland, *Nat. Commun.*, 2020, **11**, 4535.
52. N. Singh, C. Marets, J. Boudon, N. Millot, L. Saviot and L. Maurizi, *Nanoscale Advances*, 2021, **3**, 1209-1229.
53. M. Mahmoudi, *Nat. Commun.*, 2022, **13**, 49.
54. V. Francia, K. Yang, S. Deville, C. Reker-Smit, I. Nelissen and A. Salvati, *ACS Nano*, 2019, **13**, 11107-11121.
55. S. Schöttler, K. Klein, K. Landfester and V. Mailänder, *Nanoscale*, 2016, **8**, 5526-5536. View Article Online DOI: 10.1039/D3NR04862D
56. I. Alberg, S. Kramer, M. Schinnerer, Q. Hu, C. Seidl, C. Leps, N. Drude, D. Möckel, C. Rijcken and T. Lammers, *Small*, 2020, **16**, 1907574.
57. M. De, C.-C. You, S. Srivastava and V. M. Rotello, *Journal of American Chemical Society*, 2007, **129**, 10747-10753.
58. M. P. M. Soutar, L. Kempthorne, E. Annuario, C. Luft, S. Wray, R. Ketteler, M. H. R. Ludtmann and H. Plun-Favreau, *Autophagy*, 2019, **15**, 2002-2011.
59. J. C. Bae, S. H. Seo, K. Y. Hur, J. H. Kim, M. S. Lee, M. K. Lee, W. Y. Lee, E. J. Rhee and K. W. Oh, *Endocrinol. Metab.*, 2013, **28**, 26-32.
60. S. W. D. Merriel, R. Carroll, F. Hamilton and W. Hamilton, *Fam. Pract.*, 2016, **33**, 449-452.
61. W. L. Koh, P. H. Tham, H. Yu, H. L. Leo and J. C. Yong Kah, *Nanomedicine (London, England)*, 2016, **11**, 2275-2287.
62. K. Partikel, R. Korte, D. Mulac, H.-U. Humpf and K. Langer, *Beilstein Journal of Nanotechnology*, 2019, **10**, 1002-1015.
63. J. Oberländer, C. Champanhac, R. da Costa Marques, K. Landfester and V. Mailänder, *Acta Biomaterialia*, 2022, **148**, 271-278.
64. K. M. Poulsen and C. K. Payne, *Analytical and bioanalytical chemistry*, 2022, **414**, 7265-7275.
65. Y. Zou, S. Ito, F. Yoshino, Y. Suzuki, L. Zhao and N. Komatsu, *ACS Nano*, 2020, **14**, 7216-7226.
66. V. Forest and J. Pourchez, *Mater. Sci. Eng. C*, 2017, **70**, 889-896.
67. I. R. Nabi and P. U. Le, *J. Cell Biol.*, 2003, **161**, 673-677.
68. L. Billiet, J.-P. Gomez, M. Berchel, P.-A. Jaffrès, T. Le Gall, T. Montier, E. Bertrand, H. Cheradame, P. Guégan and M. Mével, *Biomaterials*, 2012, **33**, 2980-2990.
69. D. Manzanares and V. Ceña, *Pharmaceutics*, 2020, **12**.
70. L. Shen, S. Tenzer, W. Storck, D. Hobernik, V. K. Raker, K. Fischer, S. Decker, A. Dzionek, S. Krauthäuser, M. Diken, A. Nikolaev, J. Maxeiner, P. Schuster, C. Kappel, A. Verschoor, H. Schild, S. Grabbe and M. Bros, *J. Allergy Clin. Immunol.*, 2018, **142**, 1558-1570.
71. A. Acier, M. Godard, F. Gassiot, P. Finetti, M. Rubis, J. Nowak, F. Bertucci, J. L. Iovanna, R. Tomasini, P. Lécorché, G. Jacquot, M. Khrestchatisky, J. Temsamani, C. Malicet, S. Vasseur and F. Guillaumond, *Commun. Biol.*, 2021, **4**, 987.
72. E. Sehayek and S. Eisenberg, *J. Biol. Chem.*, 1991, **266**, 18259-18267.
73. I. Valladolid-Acebes, P.-O. Berggren and L. Juntti-Berggren, *Int. J. Mol. Sci.*, 2021, **22**, 932.
74. G. Rudenko, L. Henry, K. Henderson, K. Ichtchenko, M. S. Brown, J. L. Goldstein and J. Deisenhofer, *Science*, 2002, **298**, 2353-2358.
75. E. L. L. Yeo, J. U. J. Cheah, P. S. P. Thong, K. C. Soo and J. C. Y. Kah, *ACS Appl. Nano Mater.*, 2019, **2**, 6220-6229.
76. S. Patel, N. Ashwanikumar, E. Robinson, Y. Xia, C. Mihai, J. P. Griffith, S. Hou, A. A. Esposito, T. Ketova, K. Welsher, J. L. Joyal, Ö. Almarsson and G. Sahay, *Nat. Commun.*, 2020, **11**, 983.
77. S. Lara, F. Alnasser, E. Polo, D. Garry, M. C. Lo Giudice, D. R. Hristov, L. Rocks, A. Salvati, Y. Yan and K. A. Dawson, *ACS Nano*, 2017, **11**, 1884-1893.

